


# Characteristics of Minimum Variance Beamformer for Frequency and Plane-wave Compounding

Ryoya Kozai<sup>1</sup>, Norio Tagawa<sup>1</sup> <sup>a</sup>, Masasumi Yoshizawa<sup>2</sup> and Takasuke Irie<sup>1,3</sup>

<sup>1</sup>Electrical Engineering and Computer Science, Tokyo Metropolitan University, Hino-shi, Tokyo, Japan

<sup>2</sup>Tokyo Metropolitan College of Industrial Technology, Arakawa-ku, Tokyo, Japan

<sup>3</sup>Microsonic Co. Ltd., Kokubunji-shi, Tokyo, Japan

**Keywords:** Ultrasonic Imaging, Minimum Variance Beamforming, Frequency Compounding, High Resolution.

**Abstract:** Recently, coherent plane-wave compounding (CPWC) that achieves high spatiotemporal resolution has been studied actively as a spatial compounding beamformer. Further, various frequency compounding methods have been proposed for reducing speckle noise. We already proposed the method called frequency and plane-wave compounding minimum variance distortionless response (FPWC-MVDR), which achieves high spatial resolution imaging by simultaneously optimizing frequency and spatial compounding based on minimum variance scheme. In the algorithm of this method, the data-compounded-on-receive MVDR (DCR-MVDR) principle developed for CPWC is extended and applied. In this study, we analyze the features and characteristics of FPWC-MVDR and the weaknesses to be solved in the future through experiments.


## 1 INTRODUCTION

In order to realize high-resolution ultrasound imaging, it is necessary to increase the amplitude of the target signals and reduce the noise level. Beamforming is the standard method to realize it. Recent work on ultrasound beamforming has made particular progress in improving lateral resolution. Receive beamforming is the basis of array signal processing using an array transducer composed of multiple transducer elements, and is a technology that generates spatial resolution by forming the beam directivity. The most basic beamforming method is Delay-and-Sum (DAS) (Thomenius, 1996). In this method, the delays of the received signals of each element are aligned before they are added. However, this technique is strongly limited by the beamwidth, which is determined by the aperture width of the transducer array.

Various beamformings have been proposed to form narrower beams (Camacho et al., 2009), (Li and Li, 2003), (Matrone et al., 2015). Among them, much study has been done on minimum dispersion distortion-free response (MVDR) beamforming (Capon, 1969), (Vignom and Burcher, 2008), (Asl and Mahloojifar, 2012). MVDR is a method to minimize the noise power by minimizing the variance of

beamforming while guaranteeing the all-pass characteristics of the target signal. The variance can be minimized by adaptively calculating the weights for adding the received echoes using the data variance-covariance matrix. As a result, the signal level other than the target is reduced, and the improvement in lateral resolution and signal-to-noise ratio (SNR) can be expected. In a conventional system, the true variance-covariance matrix cannot be known, and it is estimated from the received echo. Therefore, various estimation methods have been proposed as approximate calculations. The most popular of these is subarray averaging (Synnevag et al., 2007). In this method, the sensor array is first divided into subarrays, and for each, the tensor product of the vectors whose components are the echoes of each subarray element is calculated. Then, a variance-covariance matrix is estimated by averaging them. However, to prevent the variance-covariance matrix from becoming singular, the subarray length must be less than half its original length. This will significantly reduce the image resolution. In addition, these processes have the disadvantage that real-time imaging is difficult due to the high computational cost.

Nguyen et al. proposed the Data-Compounded-on-Receive (DCR-MVDR) beamforming (Nguyen and Prager, 2018) to solve these problems. This is a method that efficiently applies MVDR to Coherent

<sup>a</sup>  <https://orcid.org/0000-0003-0212-9265>

Plane-Wave Compounding (CPWC) (Montaldo et al., 2009) and achieves both temporal resolution and spatial resolution. CPWC is a method that can transmit and receive plane waves while changing the angle and perform receive beamforming to obtain the same image resolution as conventional focus beam transmission in a short time. IDCR-MVDR requires a variance-covariance matrix of echoes for changes in plane wave transmit angle, which does not require subarray averaging and is calculated using a snapshot from the echo vectors received by the array. Therefore, processing can be performed without reducing the matrix size.

On the other hand, a technique called frequency compounding has also been studied as an approach to improve image quality (Magnin et al., 1982), (Mesurrolle et al., 2006), (Cui and Liu, 2011), which is a method of transmitting and receiving different frequencies in the same path and averaging them to enhance the target signal and reduce artifact echo. This takes advantage of the different interference patterns depending on the frequency. This method is mainly used for speckle reduction.

We have proposed the frequency and plane-wave compounding minimum variance distortionless response (FPWC-MVDR), which can realize high spatial resolution imaging by optimizing compounding of the frequency and plane waves simultaneously (Kozai et al., 2020). DCR-MVDR principle developed for CPWC is extended and applied to the algorithm of this method. The novelty of our approach is to optimize frequency compounding as well. Traditional frequency compounding uses a constant weighted average. However, this does not effectively use frequency information for ultrasound imaging. There may be appropriate averaging weights for each frequency, depending on the pixel position to be imaged. FPWC-MVDR has adopted an approach that optimizes frequency compounding by adaptively calculating the averaging weights. In this paper, we show various characteristics of FPWC-MVDR investigated through experiments. In particular, the trend of frequency weights offers interesting implications for future work.

## 2 METHOD

### 2.1 Minimum Variance Distortionless Response

In this paper, all observations are treated as analytic signals obtained by quadrature detection of RF sig-

nals, that is, IQ (In-phase and Quadrature-phase) signals. First, we explain MVDR using conventional sub-array averaging. Beamformer output is generally expressed by the following equation.

$$y(t) = w^H x, \quad (1)$$

where  $w$  is a weight vector,  $^H$  is Hermitian transposition, and  $x$  is a received echo vector composed of echoes acquired by all the elements, and has a time delay corresponding to the imaging position and associated phase correction. The number of elements is set to  $N$ . MVDR adaptively finds the weight vector  $w$  by solving the following constrained optimization problem (Mehdizadeh et al., 2012).

$$\text{Minimize } w^H R w, \quad \text{subject to } w^H 1_N = 1, \quad (2)$$

where  $R$  is the  $N \times N$  variance-covariance matrix.  $w$  can be obtained by solving this minimization problem and the solution is obtained as follows:

$$\hat{w} = \frac{R^{-1} 1_N}{1_N^T R^{-1} 1_N}. \quad (3)$$

In the subarray averaging process, an estimate of  $R$  is found by partitioning  $x$  into  $N - L + 1$  subarrays of length  $L$ . The estimated value  $\hat{R}$  is as follows:

$$\hat{R} = \frac{1}{N - L + 1} \sum_{l=1}^{N-L+1} x_l x_l^H, \quad (4)$$

where  $x_l \equiv [x_l, x_{l+1}, \dots, x_{l+L-1}]^T$ . By this subarray processing, the matrix size becomes  $L \times L$ , hence the size of  $w$  is also  $L$ . Therefore, the averaged echo for each subarray  $\bar{x}_l$  is defined by the following equation.

$$\bar{x}_l = \frac{1}{L} \sum_{m=l}^{l+L-1} x_m. \quad (5)$$

By using the weights of Eq. 3, the output of MVDR for each pixel  $\hat{y}$  is as follows:

$$\hat{y} = \sum_{l=1}^{N-L+1} \hat{w}_l \bar{x}_l. \quad (6)$$

### 2.2 Coherent Plane-wave Compounding

In CPWC processing, plane waves are transmitted and received multiple times at different angles. When transmitting  $M$  times at different angles and receiving with  $N$  elements, the following two-dimensional array can be generated by performing time delay and phase correction according to pixel position.

$$X = \begin{bmatrix} x_{1,1} & x_{1,2} & \cdots & x_{1,N} \\ x_{2,1} & x_{2,2} & \cdots & x_{2,N} \\ \vdots & \vdots & \ddots & \vdots \\ x_{M,1} & x_{M,2} & \cdots & x_{M,N} \end{bmatrix}, \quad (7)$$

where  $x_{i,j}$  is the echo received by element  $j$  for the pulse transmitted at the angle  $i$ . Details of the delay calculation are given in (Montaldo et al., 2009). The following CPWC output is obtained by averaging these matrix elements.

$$\hat{y}_{CPWC} = \frac{1}{MN} \sum_{i=1}^M \sum_{j=1}^N x_{i,j}. \quad (8)$$

### 2.3 Data-Compounded-on-Receive MVDR

The DCR-MVDR uses the array information and angle information of Eq. 7 because it transmits and receives while changing the angle like CPWC. The DCR-MVDR creates a snapshot from the array information and adaptively determines the angle weights without using the sub-array averaging in MVDR. The snapshot is calculated as follows:

$$s_{k,i} = \frac{1}{N-1} \sum_{j=1, j \neq k}^N x_{i,j}. \quad (9)$$

The variance-covariant matrix is defined using the snapshot of Eq. 9.

$$\hat{R}_{DCR} = \frac{1}{N} \sum_{k=1}^N s_k s_k^H + \epsilon I, \quad (10)$$

where  $\epsilon$  is the diagonal loading parameter and  $I$  is an identity matrix. Adjusting  $\epsilon$  increases the diagonal and makes the variance-covariance matrix more robust.  $\epsilon$  is set relative to  $\Delta = \text{Tr}(\hat{R})/L$ , where  $L$  is the rank of  $\hat{R}$  indicating the first term in the right hand side of Eq. 10. The signal to which the weights are applied is the vector  $u \equiv [u_1, u_2, \dots, u_M]^T$ , which is obtained by adding the matrix components of Eq. 7 in the array direction. Namely, each element  $u_i$  is computed as follows:

$$u_i = \sum_{j=1}^N x_{i,j}, \quad \text{for } i = 1, 2, \dots, M. \quad (11)$$

### 2.4 Frequency and Plane-wave Compounding-MVDR

When  $M$  times are transmitted at different angles and different frequencies are transmitted  $L$  times for each angle, and  $N$  elements are used, the third-order tensor data  $X$  can be generated (Fig. 1(a)). First, as shown in Fig. 1(a), the matrix  $Y$  for each angle is extracted and used as frequency and array information. Then, frequency weights are calculated by DCR-MVDR processing, and the weights are multiplied in the frequency direction to compress the frequency information (Fig. 1(b)). Where  $p_i (i = 1, 2, \dots, N)$  represents a

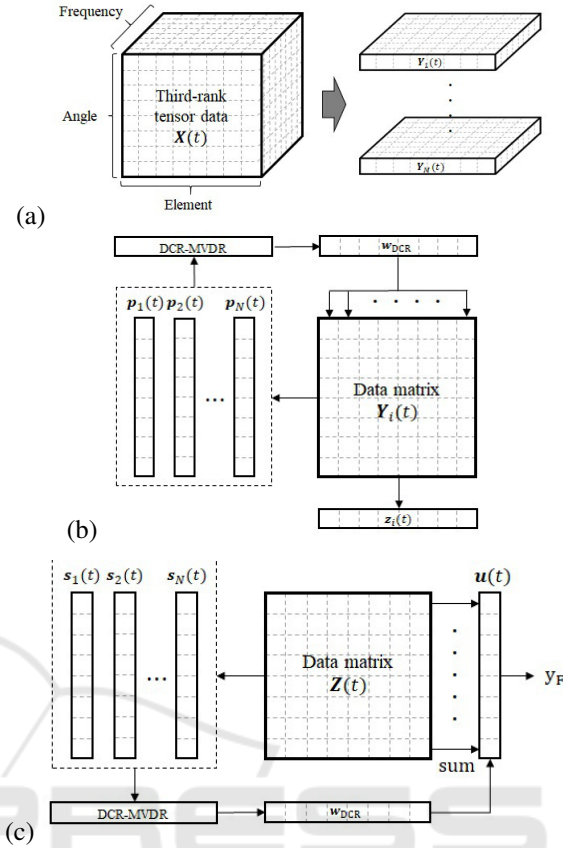


Figure 1: FPWC-MVDR processing overview: (a) partition third-order tensor data; (b) frequency compression; (c) angular weights calculation and FPWC-MVDR output.

snapshot for each transmission angle defined as Eq. 9. The matrix  $Z \equiv [z_1, z_2, \dots, z_M]$ , where  $z_i$  is generated as in Fig. 1(b), is formed by performing the above processing at all angles. Finally, by performing the same processing as DCR-MVDR on this matrix, it becomes the output of FPWC-MVDR (Fig. 1(c)).

## 3 EXPERIMENTS

### 3.1 Experiment Condition

In the experiments, the transmission and reception sequences were generated using an experimental platform for medical ultrasound (RSYS0003, Microsonic Inc., Japan) with a sampling rate of 31.25 MHz. The number of transducer elements used for both transmission and reception is 64, while the element pitch is 0.315 mm. Transmitted waves are restricted to 7-level quantization. A linear array probe (T0-1599, Nihon Dempa Kogyo Co., Ltd., Japan) was also used. The center frequency of this probe is 7.5 MHz and its spe-

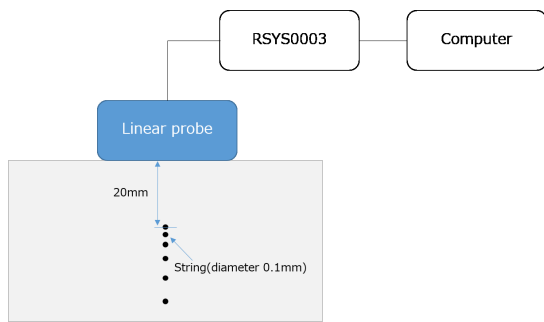


Figure 2: Experimental setting for soft tissue-mimicking phantom.

Table 1: Experimental parameters.

Parameter	Value
Transmission wave	FM-chirp pulse
Frequency band width	2 MHz
Chirp pulse duration	8 $\mu$ s
Transmission center freq.	Randomly determined at 4 – 8 MHz
Transmission voltage	60 V
Apodization	Hanning window
Measurement temperature	24 $^{\circ}$ C

cific bandwidth is 70 %. The signal processing was performed offline using MATLAB software.

Figure 2 shows the experimental setting. We present the experimental results obtained using a soft tissue-mimicking phantom (US-2 multi-purpose phantom N-365; Kyoto Kagaku Co., Ltd., Japan), with a speed of sound of 1,432 m/s (25  $^{\circ}$ C) and attenuation of 0.59 dB/cm/MHz. As shown in Fig. 2, the phantom contains six string wires with a diameter of 0.1 mm. The distances between these wires are 1.0 mm, 2.0 mm, 3.0 mm, 4.0 mm and 5.0 mm, measured from the side closest to the phantom.

Table 1 shows the experimental setting. As for transmission, plane FM-chirp waves were transmitted 33 times while changing the angle in 0.5 deg.

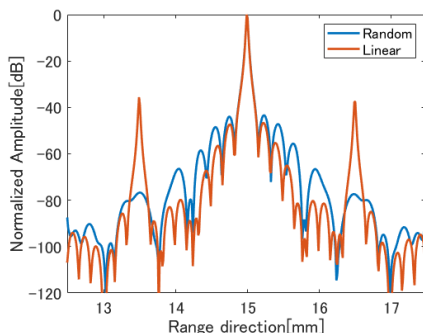


Figure 3: Comparison of intensity distribution profiles in the axial direction by regular and random changes of transmission frequency band.

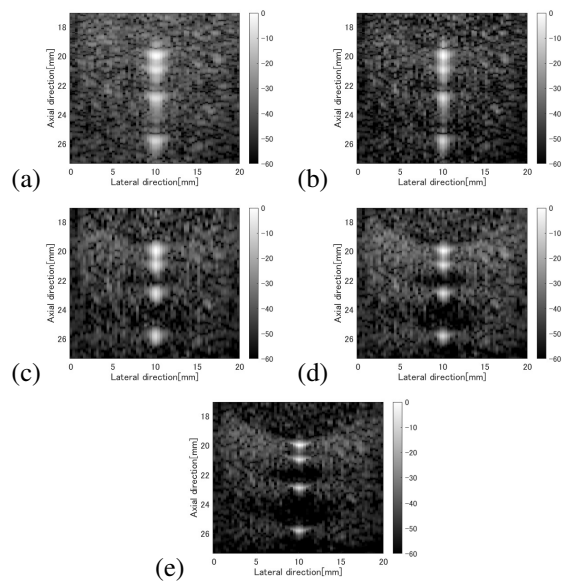


Figure 4: B-mode images when targeting string : (a) CPWC; (b) DCR-MVDR; (c) FC-DCR-MVDR; (d) FPWC-MVDR; (e) Normalized FPWC-MVDR.

steps from  $-8.0$  deg. to  $+8.0$  deg.. In addition, we changed the frequency at each angle and transmitted 8 times. 64 elements were used for transmission and reception. First, it was necessary to consider whether to change the transmission frequency band, that is, the center frequency of the transmission wave, at regular intervals or randomly. Therefore, the finite element method (FEM) simulation under almost the same transmission/reception conditions as the experiment was performed using the engineering simulation software OnScale. The object to be imaged is a thin metal wire. Figure 3 shows an example of the intensity distribution profile obtained by FPWC-MVDR using both frequency change methods. From this, it can be seen that periodic changes cause artifacts due to coherence between different frequencies. In the following, a random frequency change is adopted. In order to evaluate the performance of the frequency compounding, we also transmitted once at each angle using the total band of frequencies used. Due to the experimental system’s limitations, the pulse width is limited and is strongly affected by frequency dependent attenuation (FDA), so a relatively low frequency is used.

### 3.2 Performance Evaluation

We first evaluate the beamformer performance. Figure 4 is a comparison of B-mode images. Figure 4(a) and (b) are B-mode images of CPWC and DCR-MVDR when the total frequency band is used. Frequency Compound-DCR-MVDR (FC-DCR-MVDR)

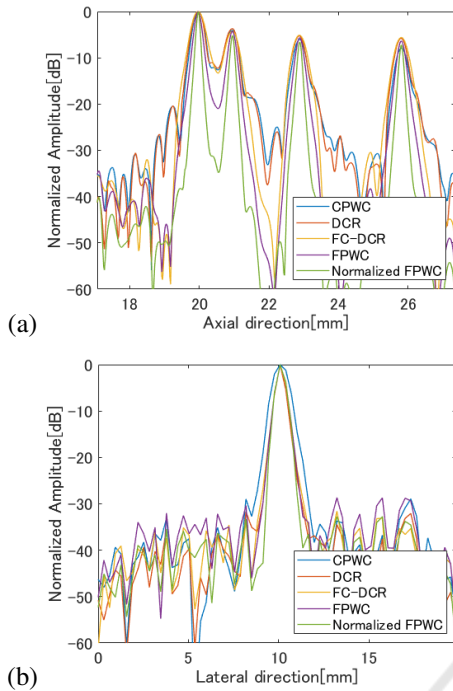


Figure 5: Intensity distribution profiles: (a) on the axial in the center of the B-mode image; (b) on the lateral line through the foremost target.

Table 2: Axial resolution at the foremost target.

Method	Axial width [mm]	
	-6 dB	-10 dB
CPWC	0.44	0.57
DCR-MVDR	0.44	0.60
FC-DCR-MVDR	0.55	0.73
FPWC-MVDR	0.37	0.53
Norm. FPWC-MVDR	0.23	0.23

in Fig. 4(c) is a method in which DCR-MVDR is combined with a frequency compounding at constant weights, and the frequency compounding is not optimized. Figure 4(d) is a result of the proposed method, FPWC-MVDR. Figure 4(e) is a B-mode image that has been FPWC-MVDR processed after the frequency dependent attenuation (FDA) compensation (Normalized FPWC-MVDR), considering that frequency information is not used effectively due to the FDA.

Table 3: Lateral resolution at the foremost target.

Method	Lateral width [mm]	
	-6 dB	-10 dB
CPWC	0.95	1.58
DCR-MVDR	0.63	0.95
FC-DCR-MVDR	0.63	0.95
FPWC-MVDR	0.63	0.95
Norm. FPWC-MVDR	0.63	0.95

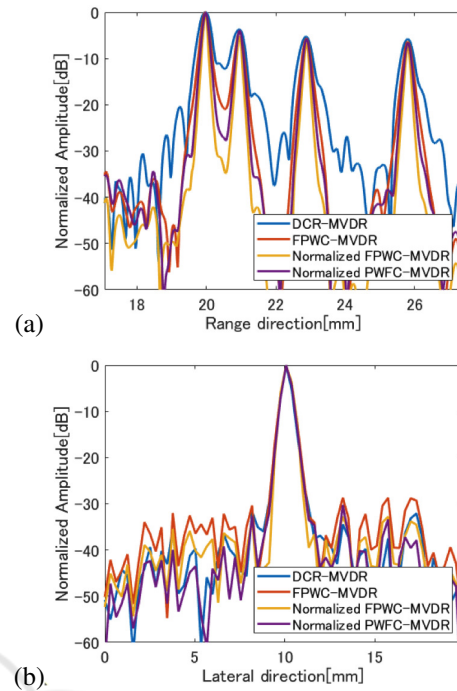


Figure 6: Intensity distribution profiles when frequency compounding is performed after plane wave compounding: (a) on the axial in the center of the B-mode image; (b) on the lateral line through the foremost target.

To check the performance in more detail, Fig. 5 shows the intensity distribution profile across the string at the foremost position. In addition, Tables 2 and 3 show the axis and lateral resolution at the foremost target. In DCR-MVDR and FC-DCR-MVDR, we set  $\epsilon = \Delta$ . In FPWC-MVDR and Normalized FPWC-MVDR, we set  $\epsilon = \Delta$  for frequency weight calculation and  $\epsilon = 2\Delta$  for angle weight calculation. These results show that frequency compounding reduces axial side lobes. In addition, it can be confirmed that FPWC-MVDR, which adaptively obtains the weights of the frequency compounding, can realize high axial resolution. We can also confirm that compensating the FDA improves its performance.

### 3.3 Other Characteristics

First, the processing order of the frequency compounding and the plane wave compounding was exchanged, and the effect was evaluated. Figure 6 shows the results of comparing the intensity profiles. In this figure, the method of conducting the plane wave compounding first is referred to as PFWC-MVDR. The results show that the PFWC-MVDR has a slightly lower axial resolution than the FPWC-MVDR, while slightly improving the lateral sidelobe level. However, since the number of transmissions with the fre-

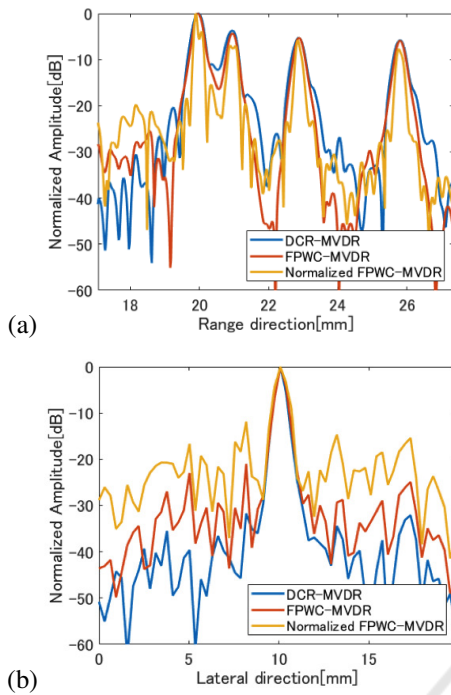


Figure 7: Intensity distribution profiles when using the entire frequency band (4-10 MHz): (a) on the axial in the center of the B-mode image; (b) on the lateral line through the foremost target.

quency changed is 8 less than the number of transmissions with the azimuth direction changed with 33, it is necessary to confirm the effect in the future.

Subsequently, DCR-MVDR, FPWC-MVDR, and Normalized FPWC-MVDR were executed using the entire effective band of 4 – 10 MHz of the used probe. The results are shown in Fig. 7. Since the frequency components of the received echo are approximately 7 MHz or less, the performance is degraded compared to the case where the 4 – 8 MHz band is used (Fig. 5). Normalized FPWC-MVDR compensates for the FDA attenuation by the normalization process, but the sidelobe increases especially in the lateral direction. Therefore, the frequency weights at the foremost target position were investigated. Comparing the weights of both determined by Normalized FPWC-MVDR shown in Fig. 8, it can be seen that the high frequency band is heavily used in the case of 4 – 10 MHz. Since the high frequency band is generally used heavily, there is a possibility that the low SNR in the high frequency band may have an adverse effect.

What is interesting about the result of these weights are that the tendency of the magnitude of the weights with respect to the frequency are V-shaped, that is, the weights are inversely proportional to the frequency in the low frequency band. An interesting

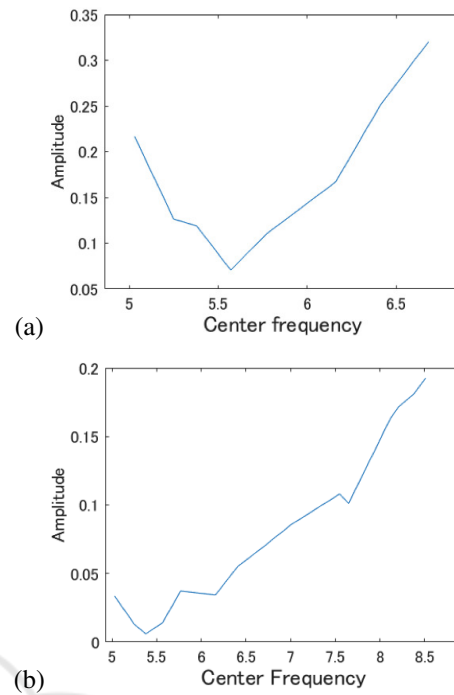


Figure 8: Absolute value of weights used for frequency compounding: (a) when using the 4 – 8 MHz band, (b) when using the 4 – 10 MHz band.

result is that lower frequencies are used more heavily than frequencies near the center. Therefore, the frequency weighting (amplitude and phase) by Normalized FPWC-MVDR was evaluated by FEM simulation using OnScale. Figure 9 shows the characteristics obtained around the target at a position of 15 mm in the axial direction and 2.24 mm in the lateral direction. From these, it can be seen that the closer to the target, the sharper the V-shape with the larger weight. It can also be confirmed that the phase of the weight is inverted with respect to the center of the entire band, but the relationship of this characteristic with the target position is not so clear.

## 4 CONCLUSIONS

In this study, we evaluated the performance and characteristics of the receive beamforming method FPWC-MVDR that we recently proposed by optimally integration of frequency and spatial compounding. Previously, we were studying methods for detecting the positions of a small number of reflectors with high resolution (Tagawa and Zhu, 2018), (Zhu and Tagawa, 2019a), (Zhu and Tagawa, 2019b), (Nguyen et al., 2020), and they were suitable for anomaly detection such as tumor imaging. On the other hand, the technical feature of these methods was to realize

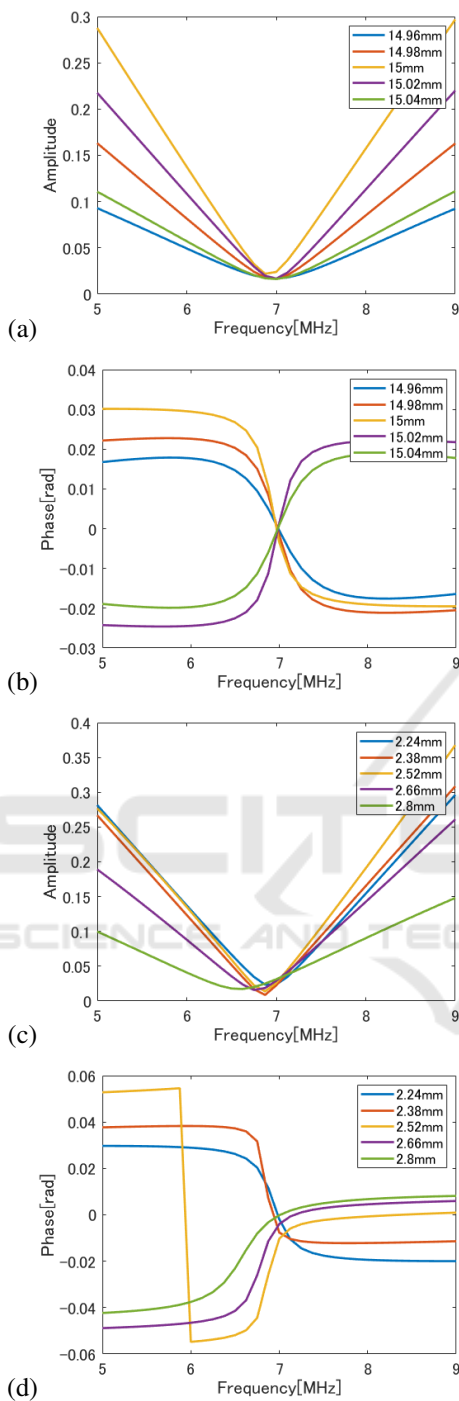


Figure 9: Differences in frequency compounding weights around the imaging target position: (a) axial weight magnitude; (b) axial weight phase; (c) lateral weight magnitude; (d) lateral weight phase.

the resolution of the wavelength level of the carrier by utilizing various frequencies for transmission and reception. The FPWC-MVDR featured in this study is also the result of applying the viewpoint of effective

use of multiple frequencies to receive beamforming.

From the evaluation results shown in this paper, it was found that the frequency characteristics of the weights used in the frequency compounding are particularly interesting. This result seems to indicate that the addition of echoes with carrier frequencies far from the center of the band is required to effectively cancel the off-axis signal. In the future, we will analyze the meaning and inevitability of the characteristics of this weight through detailed simulations and imaging experiments of various objects.

In the FPWC-MVDR, considering the reduction of the calculation amount, the echo data is first reduced in the frequency direction, the data amount is reduced, and then the plane wave transmission angle is reduced to output. If importance is placed on the optimality, it is desirable to calculate a two-dimensional weight map of frequency and transmission angle and reduce the three-dimensional tensor data at once. On the other hand, assuming a case where a high frame rate image such as a cardiac echo is required, a method capable of extracting the carrier phase more efficiently is desirable. In the frequency compounding in this study, pulses of different carrier waves were transmitted multiple times and the corresponding echoes were used. However, the FPWC-MVDR proposed in this study can also be executed by extracting and analyzing narrowband components by signal processing from the echo for one wideband transmission. We have already begun research on this method. In addition, the realization of adaptive beamforming by deep learning is effective in reducing the amount of calculation, and there are many reports (Luijten et al., 2019). This idea is also applicable to our FPWC-MVDR. We plan to proceed with further studies in terms of both computational complexity and efficiency.

Research on improving image quality by reducing speckles and noise is also being enthusiastically pursued in the field of optics (Leo et al., 2014), (Shahdoosti and Rahemi, 2019), (Jeon et al., 2018). In recent years, many studies on super-resolution technology based on deep learning have been conducted on various images (Yang et al., 2019), (Ouyang et al., 2018), (Huang et al., 2018). Based on the results there, it is important to improve the image quality of ultrasonic images from a wider perspective.

## REFERENCES

- Asl, B. M. and Mahloojifar, A. (2012). A low-complexity adaptive beamformer for ultrasound imaging using structured covariance matrix. *IEEE Trans. UFFC*, 59(4):660–667.

- Camacho, J., Parrilla, M., and Fritsch, C. (2009). Phase coherence imaging. *IEEE Trans. UFFC*, 56:958–974.
- Capon, J. (1969). High-resolution frequency-wavenumber spectrum analysis. In *Proc. IEEE*, volume 57, pages 1408–1418.
- Cui, S. and Liu, D. C. (2011). Noise reduction for ultrasonic elastography using transmit-side frequency compounding: a preliminary study. *IEEE Trans. UFFC*, 58(3):509–516.
- Huang, H., Yang, J., Huang, H., Song, Y., and Gui, G. (2018). Deep learning for super-resolution channel estimation and doa estimation based massive mimo system. *IEEE Trans. Vehicular Technology*, 67(9):8549–8560.
- Jeon, W., Jeong, W., Son, K., and Yang, H. (2018). Speckle noise reduction for digital holographic images using multi-scale convolutional neural networks. *Optics letters*, 43(17):4240–4243.
- Kozai, R., Tagawa, N., Yoshizawa, M., and Irie, T. (2020). Optimization of frequency and plane-wave compounding by minimum variance beamforming. In *IEEE Int. Ultrasonics. Symp.*
- Leo, M., Piccolo, R., Distanti, C., Memmolo, P., Paturzo, M., and Ferraro, P. (2014). Multilevel bidimensional empirical mode decomposition: a new speckle reduction method in digital holography. *Optical Engineering*, 53(11):112314–1–10.
- Li, P. C. and Li, M. L. (2003). Adaptive imaging using the generalized coherence factor. *IEEE Trans. UFFC*, 50:128–142.
- Luijten, B., Cohen, R., de Bruijn, F. J., Schmeitz, H. A. W., Mischi, M., Eldar, Y. C., and van Israel, R. J. G. (2019). Deep learning for fast adaptive beamforming. In *IEEE Int. Conf. Acoust. Speech and Signal Process.*, pages 1333–1337.
- Magnin, P. A., von Ramm, O. T., and Thurstone, F. L. (1982). Frequency compounding for speckle contrast reduction in phased array images. *Ultrasonic imaging*, 4(3):267–281.
- Matrone, G., Savoia, S. A., Caliano, G., and Magenes, G. (2015). The delay multiply and sum beamforming algorithm in ultrasound b-mode medical imaging. *IEEE Trans. Med. Imag.*, 34(4):940–949.
- Mehdizadeh, S., Austeng, A., Johansen, T. F., and Holm, S. (2012). Eigenspace based minimum variance beamforming applied to ultrasound imaging of acoustically hard tissues. *IEEE Trans. Med. Imag.*, 31(10):1912–1921.
- Mesurolle, B., Bining, H. J., Khoury, M. E., Barhdadi, A., and Kao, E. (2006). Contribution of tissue harmonic imaging and frequency compound imaging in interventional breast sonography. *Journal of ultrasound in medicine*, 25(7):845–855.
- Montaldo, G., Tanter, M., Bercoff, J., Benech, N., and Fink, M. (2009). Coherent plane-wave compounding for very high frame rate ultrasonography and transient elastography. *IEEE Trans. UFFC*, 56(3):489–506.
- Nguyen, C. H., Tagawa, N., Yoshizawa, M., and Irie, T. (2020). Performance improvement of ultrasonic range super-resolution based on phase rotation by dealing with echo distortion. *Proc. of Meeting on Acoust. (POMA)*, 38:055009–1–13.
- Nguyen, N. Q. and Prager, R. W. (2018). A spatial coherence approach to minimum variance beamforming for plane-wave compounding. *IEEE Trans. UFFC*, 65(4):522–534.
- Ouyang, W., Aristov, A., Lelek, M., Hao, X., and Zimmer, C. (2018). Deep learning massively accelerates super-resolution localization microscopy. *Nature Biotechnology*, 36:460–468.
- Shahdoosti, H.-R. and Rahemi, Z. (2019). Edge-preserving image denoising using a deep convolutional neural network. *Signal Processing*, 159:20–32.
- Synnevag, J. F., Austeng, A., and Holm, S. (2007). Adaptive beamforming applied to medical ultrasound imaging. *IEEE Trans. UFFC*, 54(8):1606–1613.
- Tagawa, N. and Zhu, J. (2018). Super-resolution ultrasound imaging based on the phase of the carrier wave without deterioration by grating lobes. In *Int. Conf. Pattern Recog.*, pages 2791–2796.
- Thomenius, K. E. (1996). Evolution of ultrasound beamformers. In *IEEE Int. Ultrason. Symp.*, volume 2, pages 1615–1622.
- Vignom, F. and Burcher, M. R. (2008). Capon beamforming in medical ultrasound imaging with focused beams. *IEEE Trans. UFFC*, 55:619–628.
- Yang, W., Zhang, X., Tian, Y., Wang, W., Xue, J.-H., and Liao, Q. (2019). Deep learning for single image super-resolution: A brief review. *IEEE Trans. Multimedia*, 21(12):3106–3121.
- Zhu, J. and Tagawa, N. (2019a). High resolution ultrasonic imaging based on frequency sweep in both of transducer element domain and imaging line domain. *Jpn. J. Appl. Phys.*, 58:SGGE03–1–7.
- Zhu, J. and Tagawa, N. (2019b). Improvement of performance degradation in synthetic aperture extension of enhanced axial resolution ultrasound imaging based on frequency sweep. *Sensors*, 19:2414–1–18.